A R C H I V E O F M E C H A N I C A L E N G I N E E R I N G

Volume 66 2019 Number 3

DOI: 10.24425/ame.2019.129676

Key words: phase change, natural convection, extended finite element method, level set method

Paweł Stąpór [1]

The modified XFEM for solving problems of a phase change with natural convection

This paper presents an extended finite element method applied to solve phase change problems taking into account natural convection in the liquid phase. It is assumed that the transition from one state to another, e.g., during the solidification of pure metals, is discontinuous and that the physical properties of the phases vary across the interface. According to the classical Stefan condition, the location, topology and rate of the interface changes are determined by the jump in the heat flux. The incompressible Navier–Stokes equations with the Boussinesq approximation of the natural convection flow are solved for the liquid phase. The no-slip condition for velocity and the melting/freezing condition for temperature are imposed on the interface using penalty method. The fractional four-step method is employed for analysing conjugate heat transfer and unsteady viscous flow. The phase interface is tracked by the level set method defined on the same finite element mesh. A new combination of extended basis functions is proposed to approximate the discontinuity in the derivative of the temperature, velocity and the pressure fields. The single-mesh approach is demonstrated using three two-dimensional benchmark problems. The results are compared with the numerical and experimental data obtained by other authors.

1. Introduction

Phase change processes play an important role in a number of industry-related applications, including casting in metallurgy, heat storage systems, cryosurgery, food conservation, diffusion of gases in biological tissues or penetration of solvents in polymers. Solidification is also present in various natural processes, for example, iceberg evolution, magma chamber evolution or crust formation. The modelling of

✉ P. Stąpór, e-mail: stapor@tu.kielce.pl

[1]Faculty of Management and Computer Modelling, Kielce University of Technology, Kielce, Poland.

such problems is still a challenging task for the materials engineering and science communities. A comprehensive review of the transport phenomena in multi-phase systems is presented in [1]. In [2] and [3] the authors discuss the basic concepts of solidification processes and propose their mathematical modelling. The finite-element method used for fluid dynamics is discussed extensively in [4].

The simplified models consider heat conduction as a principal way of energy transport during material melting/solidification. Natural convection during freezing of water is an example of a phase change system where the phenomena cannot be neglected. Recent practical applications of phase-change materials (PCMs) to energy-storage systems show the crucial role of natural convection in heat transfer and the propagation of the interface between the phases. Accordingly, the model needs to take into account flow in the liquid phase.

A variety of numerical techniques can be applied to obtain an approximate solution to a phase change problem. The approaches are based either on the deforming grid (interface tracking) methods or the fixed grid (interface capturing) methods. The deforming grid schemes use a transformed coordinate system, obtained by performing complicated mathematical operations, to find the position of the interface explicitly. When the finite element method (FEM) is applied, the shape of the mesh needs to correspond to that of the interface, and the problem is solved separately for each domain, [5, 6]. The major drawback of this method is that remeshing and field mapping must be performed every few discrete time steps, which is due to the unacceptable distortion of the original mesh. In the fixed grid schemes, on the other hand, discontinuities are smoothed across a certain distance instead of being treated accurately (enthalpy approach), [7–9].

The partition of unity (PU) concept can be employed to enrich the classical FEM with specific information about the solution, [10]. The local information can be added directly to the finite element approximation; this, however, requires that the method be controlled through additional elemental degrees of freedom, [11]. The extended finite element method (XFEM) allows one to enrich the approximation through additional nodal shape functions. The XFEM was used successfully in [12] to analyse crack propagation problems. Merle and Dolbow [13] and Chessa et al., [14] were some of the first to apply the XFEM to solve phase change problems. In [15], the author formulates the one-dimensional phase change problem for a system with thermo-dependent properties and solves it using the XFEM combined with the Newton-Raphson method. In [16], authors consider the use of the XFEM to describe dendritic solidification with melt convection. They use a diffused-interface model to solve the momentum equations, where the interface is smeared out over a region. Enrichment is used only to solve the thermal problem. The simulation of solidification processes with arbitrary flow in the liquid part is considered in [17], where XFEM is used in the analysis of the physically non-linear problem. In [18, 19], authors employ the XFEM to analyse a two-phase flow, which, computationally, is a similar problem. They solve the Navier-Stokes equations and use abs-enrichment to account for the kink in the

velocity field. The jump in pressure is not considered. Recently, Li et al. [20] and Martin et al. [21] consider the XFEM method to solve two-dimensional solidification problems including natural convection. They use abs-enrichment scheme for the temperature approximation, while the sign-enrichment scheme for the melt velocity and pressure. Constraints at the interface, such as interface temperature and non-slip condition, are imposed by the penalty method or Lagrange multiplier approach.

In this paper, the XFEM is applied to solve problems of a phase change with natural convection in the liquid phase. The proposed enrichment scheme, used in the momentum equations, is different to those previously mentioned what allows for better approximation of the velocity field near the interface. The mathematical model of the problem is represented by the incompressible Navier–Stokes equations combined with the Boussinesq approximation of the natural convection flow. It is assumed that the physical properties of the phases vary across the interface. The fractional four-step method for analysing conjugate heat transfer and unsteady viscous flow is applied to solve the equations. The no-slip condition for velocity and the melting/freezing condition for temperature are imposed on the interface using the penalty method. A new combination of extended basis functions is employed to approximate the discontinuity in the velocity and the pressure fields. It is assumed that the solidification front changes over time and the rate is dependent on the jump in the heat flux across the interface, according to the classical Stefan condition. The phase interface is captured by the level set method (LSM), defined on the same finite element mesh.

The LSM was introduced by Osher and Sethian [22]. In its implicit form, it can be used extensively to deal with various problems, including the movement of the interface resulting in the separation of two or more regions, e.g., crack propagation, [23], multi-phase flow, [24], shape optimization, [25], flame modelling, [26] or image processing, [27], to mention just a few.

The proposed single-mesh approach is demonstrated on two-dimensional benchmark problems. The simulation results are compared with the experimental data and simulation results obtained with other methods.

The structure of the paper is as fallows. The problem considered throughout the paper, i.e., the solidification/melting of a material in a two-dimensional space, is defined in Section 2. The model includes the natural convection in the liquid phase. Section 3 discusses the application of the LSM to track the position of the interface independently of the temperature field. Section 4 gives a brief overview of the main features of the XFEM and proposes a new combination of enrichment functions. The resulting matrix equations are provided in Section 5. Section 6 describes the penalty method used to enforce the interface conditions, and finally, Section 7 presents the calculation results for the selected two-dimensional problems. Three cases are considered: natural convection of water in a square cavity without a phase change, water freezing with natural convection and melting of a phase-change material.

2. Formulation of the problem

2.1. Assumptions

Let us consider a two-dimensional domain Ω with boundary Γ divided into the solid region Ω_S and the liquid region Ω_L, respectively (Fig. 1). The interface Γ_I separates liquid and solid sub-domains. The external boundary Γ contains of the parts Γ_D and Γ_N such that $\Gamma = \Gamma_D \cup \Gamma_N$ and $\Gamma_D \cap \Gamma_N = \emptyset$. The vectors $\mathbf{n}$ and $\mathbf{n}_I$ define normal vectors on the external boundary Γ and the interface boundary Γ_I, respectively.

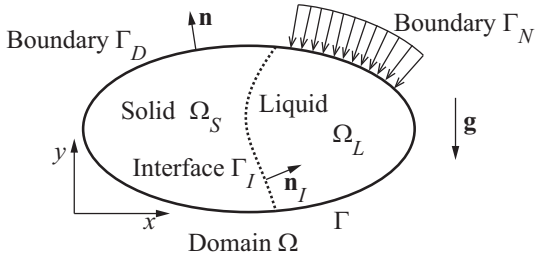

Fig. 1. Domain Ω split into Ω_L and Ω_S by the interface Γ_I

The velocity and the pressure at the point $\mathbf{x}$ in Ω_L and at the time t are $\mathbf{u}(\mathbf{x}, t)$ and $p(\mathbf{x}, t)$, respectively. It is assumed that $\mathbf{u}(\mathbf{x}, t) = \mathbf{0}$ inside Ω_S and the no-slip boundary condition is held at the external boundary Γ and at the interface Γ_I. The temperature at the point $\mathbf{x}$ in Ω and at the time t is $T(\mathbf{x}, t)$. The temperature boundary conditions define the Dirichlet condition prescribed at part of the boundary Γ_D and the Neumann condition defined at Γ_N.

The densities of the solid and the liquid phases can differ; however, there is no material transport due to expansion or shrinkage caused by a phase change. The heat can be transferred by conduction in the solid part and by conduction and convection in the liquid part. The convection in the liquid is a result of the buoyancy-driven flow. The material properties change discontinuously across the interface. The incompressible flow and isotropy with respect to heat conduction are another assumption, which completes the formulation of the problem.

2.2. Governing equations

The convection-diffusion heat equation governs the temperature $T(\mathbf{x}, t)$ in both liquid and solid parts of Ω

$$c\left(\frac{\partial T(\mathbf{x}, t)}{\partial t} + \mathbf{u}(\mathbf{x}, t) \cdot \nabla T(\mathbf{x}, t)\right) = k\nabla^2 T(\mathbf{x}, t) + f \quad \text{in } \Omega \times J, \tag{1}$$

where c, k, f denote the volumetric specific heat capacity, the thermal conductivity and a heat source, respectively. The velocity field $\mathbf{u}$ fulfils the condition: $\mathbf{u} = \mathbf{0}$ in Ω_S, and $J = (0, t]$ ($t > 0$) is the time interval of interest.

The coefficients c and k are discontinuous across the interface boundary Γ_I

$$c = \begin{cases} c_L = \rho_L \cdot c_L^p & \text{in } \Omega_L, \\ c_S = \rho_S \cdot c_S^p & \text{in } \Omega_S, \end{cases} \qquad k = \begin{cases} k_L & \text{in } \Omega_L, \\ k_S & \text{in } \Omega_S, \end{cases} \tag{2}$$

where c_L^p, c_S^p are the specific heat capacities of the liquid and the solid phases, and ρ_L, ρ_S are their material densities.

The temperature on the external boundary Γ_D and the heat flux on Γ_N are given

$$T(\mathbf{x}, t) = T_D(\mathbf{x}, t) \quad \text{at } \Gamma_D \times J, \tag{3}$$

$$-k\nabla T(\mathbf{x}, t) \cdot \mathbf{n} = q_N(\mathbf{x}, t) \quad \text{at } \Gamma_N \times J. \tag{4}$$

The temperature in Ω at $t = 0$ defines the initial condition

$$T(\mathbf{x}, 0) = T_0(\mathbf{x}) \quad \text{in } \Omega. \tag{5}$$

The *internal condition* has to be satisfied at the interface boundary Γ_I

$$T(\mathbf{x}, t) = T_M \quad \text{at } \Gamma_I, \tag{6}$$

where T_M is the melting/solidification temperature.

The *Stefan condition* resulting from the energy conservation across the surface Γ_I, as described in [28], has the form

$$\rho_S \left(\ell^p + (c_L - c_S)(T_M - T_M^*) \right) V_I + \frac{\rho_S}{2} \left(1 - \frac{\rho_S}{\rho_L} \right)^2 V_I^3 = \bar{q} \quad \forall \mathbf{x} \in \Gamma_I, \tag{7}$$

where $\bar{q}$, ℓ^p, T_M^* and V_I are the jump in the heat flux at the interface, the latent heat of fusion, the bulk melting temperature and the normal velocity of the interface, respectively. In the case when the cubic term is negligibly small and fusion temperature is constant, the condition (7) takes the simpler form

$$V_I(\mathbf{x}, t) = \frac{\bar{q}(\mathbf{x}, t)}{\ell} \quad \forall \mathbf{x} \in \Gamma_I, \tag{8}$$

where $\ell = \ell^p \rho_S$.

The jump in the heat flux at the interface is calculated according to

$$\bar{q}(\mathbf{x}, t) = (k_S \nabla T(\mathbf{x}, t)|_{\Gamma_I^S} - k_L \nabla T(\mathbf{x}, t)|_{\Gamma_I^L}) \cdot \mathbf{n}_I, \tag{9}$$

where Γ_I^S is the solid side and Γ_I^L is the liquid side of the interface Γ_I.

The fluid velocity $\mathbf{u}(\mathbf{x}, t)$ and pressure $p(\mathbf{x}, t)$ in Ω_L are governed by the *Navier-Stokes* equations in the velocity-pressure formulation

$$\begin{gathered}\frac{\partial \mathbf{u}(\mathbf{x}, t)}{\partial t} + \mathbf{u}(\mathbf{x}, t) \cdot \nabla \mathbf{u}(\mathbf{x}, t) - \nu \nabla^2 \mathbf{u}(\mathbf{x}, t) + \frac{1}{\rho_L} \nabla p(\mathbf{x}, t) = \mathbf{f} \quad \text{in } \Omega_L \times J, \\ \nabla \cdot \mathbf{u}(\mathbf{x}, t) = 0 \quad \text{in } \Omega_L \times J,\end{gathered} \tag{10}$$

where ν and $\mathbf{f}$ are the kinematic viscosity and applied body force, respectively.

Equations (10) describe the motion of a nonstationary, isothermal and incompressible Newtonian fluid. The Dirichlet boundary conditions at the boundary Γ of the domain Ω_L are given

$$\mathbf{u}(\mathbf{x}, t) = \mathbf{u}_D(\mathbf{x}, t) \quad \text{at } \Gamma \in \Omega_L \times J. \tag{11}$$

The no-slip boundary condition is prescribed at the interface Γ_I

$$\mathbf{u}(\mathbf{x}, t) = \mathbf{B} \quad \text{at } \Gamma_I \times J. \tag{12}$$

The divergence-free initial velocity field in Ω_L closes the problem

$$\mathbf{u}(\mathbf{x}, 0) = \mathbf{u}_0(\mathbf{x}) \quad \text{in } \Omega_L\,. \tag{13}$$

The velocity and the pressure in $\Omega_S$are assumed to be equal to zero.

The buoyancy-driven flow is introduced using the Boussinesq approximation. In the approximation, the variation in density is neglected, except in the body force term. The corresponding buoyancy force is then defined as

$$\mathbf{f} = \frac{1}{\rho_L}(\rho(T) - \rho_0)\mathbf{g}, \tag{14}$$

where $\mathbf{g}$ is the gravitational force and ρ_0 is the reference density.

If the dependence of the density on the temperature is linear, the buoyancy term is reduced to

$$\mathbf{f} = \beta(T_0 - T)\mathbf{g}, \tag{15}$$

where β is the coefficient of expansion for the fluid and T_0 is the reference temperature.

The system of the Navier-Stokes equations (10) and (1) with the initial and boundary conditions completes the mathematical formulation of the problem.

3. Level set method

The level set method requires that the moving interface $\Gamma_I(t)$ be modelled as a zero-level set of a higher-dimensional surface $\phi(t)$ such that

$$\Gamma_I(t) = \{\mathbf{x}\colon \phi(\mathbf{x}, t) = 0\}. \tag{16}$$

The evaluation of the time dependent level set function ϕ for the velocity field $\mathbf{u}_\phi$ is governed by the *level set equation*

$$\frac{\partial \phi(\mathbf{x},t)}{\partial t} + \mathbf{u}_\phi \cdot \nabla \phi(\mathbf{x},t) = 0 \quad \text{in } \Omega \times J \tag{17}$$

with the initial condition

$$\phi(\mathbf{x},0) = \phi_0(\mathbf{x}). \tag{18}$$

A signed distance function is used as level set function ϕ

$$\phi(\mathbf{x},t) = \pm \min_{\mathbf{x}_I \in \Gamma_I} \|\mathbf{x} - \mathbf{x}_I\| \quad \forall \mathbf{x} \in \Omega. \tag{19}$$

Thus, the normal vector $\mathbf{n}_I$ can be obtained at any point of the domain with the following formula

$$\mathbf{n}_I(\mathbf{x}) = \frac{\nabla \phi(\mathbf{x},t)}{\|\nabla \phi(\mathbf{x},t)\|}. \tag{20}$$

The level set method assumes that the convective velocity field $\mathbf{u}_\phi$ is known in the entire domain Ω. Since the Stefan condition defines the normal velocity only at the interface, some technique must be used in order to find it in the domain, [29]. According to the method proposed in [14], the solution of partial differential equation

$$\operatorname{sign}(\phi(\mathbf{x}))\nabla V(\mathbf{x}) \cdot \nabla \phi(\mathbf{x}) = 0 \quad \text{in } \Omega \tag{21}$$

with condition

$$V(\mathbf{x}) = V_I(\mathbf{x}) \quad \text{at } \mathbf{x} \in \Gamma_I \tag{22}$$

provides orthogonal extension of V_I

$$\mathbf{u}_\phi(\mathbf{x}) = V(\mathbf{x})\mathbf{n}_I(\mathbf{x}). \tag{23}$$

The solution of equation (21) with finite elements methods needs a weak formulation

$$(\operatorname{sign}(\phi_h)\nabla V_h \cdot \nabla \phi_h, v_h) + (\lambda \nabla \phi_h \cdot \nabla v_h, \nabla V_h \cdot \nabla \phi_h) = 0 \quad \forall v_h \in V_h\,. \tag{24}$$

where $(\cdot,\cdot)$ denotes the L_2 inner product over the domain Ω_h, V_h is a finite element subspace of the test function v_h and λ is a stabilization parameter, [30].

Thus, the matrix form of equation (24) with approximation of V_h and ϕ_h is

$$\mathbf{K}\,\mathbf{V} = \mathbf{0}, \tag{25}$$

where

$$\mathbf{K} = \int_{\Omega_h} \operatorname{sign}(\mathbf{N}\phi)\mathbf{N}^{\mathrm{T}}\phi^{\mathrm{T}}\nabla\mathbf{N}^{\mathrm{T}}\nabla\mathbf{N}\,\mathrm{d}\Omega_h + \int_{\Omega_h} \lambda\nabla\mathbf{N}^{\mathrm{T}}\nabla\mathbf{N}\phi\,\phi^{\mathrm{T}}\nabla\mathbf{N}^{\mathrm{T}}\nabla\mathbf{N}^{\mathrm{T}}\,\mathrm{d}\Omega_h\,, \tag{26}$$

with the vector of the elemental shape functions and the level set degrees of freedom being $\mathbf{N} = \mathbf{N}(\mathbf{x})$ and ϕ, respectively.

In this study, the boundary condition (22) is used, according to the approach proposed in [30], where the velocity of the interface is projected to the nodes of elements containing the interface. The solution of equation (25) with boundary condition (22) allows one to find the velocity field $\mathbf{u}_\phi$ at any point $\mathbf{x}$ in Ω

$$\mathbf{u}_\phi(\mathbf{x}) = \mathbf{N}(\mathbf{x})\mathbf{V}\,\mathbf{n}_I(\mathbf{x}). \tag{27}$$

The weak formulation of the level set equation (17) with a stabilization term is given by

$$\begin{gathered}\left(\frac{\partial \phi_h}{\partial t}, v_h\right) + \left(\frac{\partial \phi_h}{\partial t}, \lambda \mathbf{u}_\phi \cdot \nabla v_h\right) + \left(\mathbf{u}_\phi \cdot \nabla \phi_h, v_h\right) + \left(\mathbf{u}_\phi \cdot \nabla \phi_h, \lambda \mathbf{u}_\phi \cdot \nabla v_h\right) = 0, \\ (\phi_h(\cdot, 0), v_h) = (\phi_0, v_h) \quad \forall v_h \in V_h\,.\end{gathered} \tag{28}$$

The finite element equation is obtained after the approximation of ϕ_h and v_h is introduced to formula (28)

$$\begin{gathered}\mathbf{C}_\phi \frac{\mathrm{d}\phi}{\mathrm{d}t} + \mathbf{B}_\phi \phi = \mathbf{B} \quad t \in J, \\ \phi(0) = \phi_0\,.\end{gathered} \tag{29}$$

Since the problem is time-dependent, an explicit time integration scheme is applied

$$\frac{1}{\Delta t}\mathbf{C}_\phi \phi^n = \left(\frac{1}{\Delta t}\mathbf{C}_\phi - \mathbf{B}_\phi\right)\phi^{n-1}, \tag{30}$$

where

$$\mathbf{C}_\phi = \int_{\Omega_h} \mathbf{N}^{\mathrm{T}}\mathbf{N} + \lambda \nabla \mathbf{N}^{\mathrm{T}} \mathbf{u}_\phi^{\mathrm{T}} \nabla \mathbf{N}\, \mathrm{d}\Omega_h\,, \tag{31}$$

$$\mathbf{B}_\phi = \int_{\Omega_h} \mathbf{N}^{\mathrm{T}}\mathbf{u}_\phi \nabla \mathbf{N} + \lambda \nabla \mathbf{N}^{\mathrm{T}} \mathbf{u}_\phi^{\mathrm{T}} \mathbf{u}_\phi \nabla \mathbf{N}\, \mathrm{d}\Omega_h\,. \tag{32}$$

4. Extended finite element method

If it is generally assumed that the thermal properties and viscosity are discontinuous across the interface, there is a kink in the temperature and velocity fields and so is a jump in the pressure field.

In the XFEM, a special approximation is applied by extending the continuous approximation $U(\mathbf{x})_C$ with discontinuous (enriched) term $U(\mathbf{x}, \mathbf{x}_I)_E$

$$U_h(\mathbf{x}) = U(\mathbf{x})_C + U(\mathbf{x}, \mathbf{x}_I)_E\,, \tag{33}$$

where

$$U(\mathbf{x})_C = \sum_{i \in I} N_i(\mathbf{x}) U_i \tag{34}$$

and U is a solution function. The discontinuous term $U(\mathbf{x}, \mathbf{x}_I)_E$ is a combination of enrichment function $\Psi^\alpha(\mathbf{x}, \mathbf{x}_I)$ and usually element shape functions $\mathbf{N}(\mathbf{x})$

$$U(\mathbf{x}, \mathbf{x}_I)_E = \sum_{j \in J} \sum_{\alpha=1}^{m} N_j(\mathbf{x}) \Psi^\alpha(\mathbf{x}, \mathbf{x}_I) a_j^\alpha , \tag{35}$$

where J indicates the nodes enriched with $\Psi^\alpha(\mathbf{x}, \mathbf{x}_I)$, a_j^α are the enriched degrees of freedom, I is the total number of nodes and m is the number of enrichment functions and $\mathbf{x}_I$ denotes that the term depends on the position of the interface.

A compact form of the approximation (33) is given by

$$U_h(\mathbf{x}) = \mathbf{N}_{\mathrm{U}}(\mathbf{x}, \mathbf{x}_I) \mathbf{U}_{\mathrm{X}} , \tag{36}$$

where $\mathbf{N}_{\mathrm{U}}$ is a vector of enriched shape functions and $\mathbf{U}_{\mathrm{X}}$ is the extended degrees of freedom vector

$$\begin{aligned} \mathbf{N}_{\mathrm{U}}(\mathbf{x}, \mathbf{x}_I) &= \begin{bmatrix} \mathbf{N}(\mathbf{x}) & \mathbf{N}(\mathbf{x}) \boldsymbol{\Psi}_{\mathrm{j}}(\mathbf{x}, \mathbf{x}_I) \end{bmatrix}, \\ \mathbf{U}_{\mathrm{X}} &= \begin{bmatrix} \mathbf{U} \\ \mathbf{a}_j \end{bmatrix}. \end{aligned} \tag{37}$$

As the nodal values of the level set function $\phi(\mathbf{x}_i)$ are known, the set of enriched nodes J can be easily found according to

$$J = \left\{ k \in \{1, \ldots, e\} \colon \min_{i \in I_k^e} (\phi(\mathbf{x}_i)) \cdot \max_{i \in I_k^e} (\phi(\mathbf{x}_i)) < 0 \right\}, \tag{38}$$

where I_k^e is the set of nodes belonging to the element e.

The extended finite element mesh includes the standard elements, reproducing elements (the elements cut by the interface) and blending elements (elements partially enriched). Since the approximation in the partially enriched elements does not fulfil a partition of unity property, several techniques are proposed to improve the convergence and accuracy of the method [31, 32].

This study proposes special enrichment functions that vanish in blending elements; as a result, the optimal convergence rate can be achieved. The approximation of the temperature field is enriched using the abs-enrichment function proposed by Moës et al. [33]

$$\Psi(\mathbf{x}) = \mathbf{N}(\mathbf{x}) |\phi| - |\mathbf{N}(\mathbf{x})\, \phi| . \tag{39}$$

The Heaviside (step) function is used to determine the strong discontinuity in the pressure field. The function is represented as

$$H(\mathbf{x}) = \begin{cases} -1 & \text{if } \phi(\mathbf{x}) < 0, \\ +1 & \text{if } \phi(\mathbf{x}) \geqslant 0. \end{cases} \tag{40}$$

Applying the *shifted-basis* approximation, [34, 35] leads to the following formula

$$\Psi_j^p(\mathbf{x}) = H(\mathbf{x}) - H(\mathbf{x}_j). \tag{41}$$

In the blending elements, the Heaviside function (40) has the same value at each point of the element, which means that the function (41) vanishes for this type of elements.

The kink in the velocity field is approximated using two types of enrichment functions proposed originally in the analysis of the Poisson equation with discontinuous coefficient by Stąpór [36]

$$\Psi^1(\mathbf{x}) = \Psi(\mathbf{x}) \tag{42}$$

and

$$\Psi_j^2(\mathbf{x}) = \Psi(\mathbf{x})\frac{1 + H(\mathbf{x})H(\mathbf{x}_j)}{2\mathbf{N}(\mathbf{x})|\phi|} + \frac{1 - H(\mathbf{x})H(\mathbf{x}_j)}{2}. \tag{43}$$

Since $\Psi(\mathbf{x}) = 0$ and $H(\mathbf{x})H(\mathbf{x}_j) = 1$, the enrichment term (43) is not active in the blending elements. The proposed enrichment functions can be used to eliminate a spurious deviation of velocity in the vicinity of the interface. When the standard abs-enrichment is applied, unphysical oscillations occur because the standard approximation cannot compensate for the quadratic terms if the solution is linear or constant in any part of the enriched region.

5. Temporal and spatial discretizations

The fractional four-step method proposed in [37] and the second order Crank-Nicolson scheme are applied to the momentum and continuity equations (10). The finite element equations are based on the weak Galerkin formulation of the corresponding differential equation. Details of the derivation of the weak formulation are provided in [38].

In the first step of the approach, an intermediate velocity field $\hat{\mathbf{u}}_{\mathrm{X}}^n$ is obtained by solving the momentum equation

$$\left(\frac{1}{\Delta t}\mathbf{C} + \frac{1}{2}(\mathbf{B} + \mathbf{A})\right)\hat{\mathbf{u}}_{\mathrm{X}}^n = \left(\frac{1}{\Delta t}\mathbf{C}^* - \frac{1}{2}(\mathbf{B}^* + \mathbf{A}^*)\right)\mathbf{u}_{\mathrm{X}}^{n-1} - \mathbf{G} + \mathbf{R}, \tag{44}$$

where n defines the time step. The matrices and vectors are defined as follows

$$\mathbf{C} = \int_{\Omega_h} \mathbf{N}_{\mathrm{u}}^{\mathrm{T}}(\mathbf{x}, \mathbf{x}_I^n)\mathbf{N}_{\mathrm{u}}(\mathbf{x}, \mathbf{x}_I^n)\,\mathrm{d}\Omega_h\,, \tag{45}$$

$$\mathbf{C}^* = \int_{\Omega_h} \mathbf{N}_{\mathrm{u}}^{\mathrm{T}}(\mathbf{x}, \mathbf{x}_I^n)\mathbf{N}_{\mathrm{u}}(\mathbf{x}, \mathbf{x}_I^{n-1})\,\mathrm{d}\Omega_h\,, \tag{46}$$

$$\mathbf{B} = \int_{\Omega_h} \mathbf{N}_{\mathrm{u}}^{\mathrm{T}}(\mathbf{x}, \mathbf{x}_I^n)\mathbf{u}^{n-1}\nabla\mathbf{N}_{\mathrm{u}}(\mathbf{x}, \mathbf{x}_I^n)\,\mathrm{d}\Omega_h\,, \tag{47}$$

$$\mathbf{B}^* = \int_{\Omega_h} \mathbf{N}_{\mathrm{u}}^{\mathrm{T}}(\mathbf{x}, \mathbf{x}_I^n)\mathbf{u}^{n-1}\nabla\mathbf{N}_{\mathrm{u}}(\mathbf{x}, \mathbf{x}_I^{n-1})\,\mathrm{d}\Omega_h\,, \tag{48}$$

$$\mathbf{A} = \int_{\Omega_h} \nu\nabla\mathbf{N}_{\mathrm{u}}^{\mathrm{T}}\mathbf{x}, \mathbf{x}_I^n)\nabla\mathbf{N}_{\mathrm{u}}(\mathbf{x}, \mathbf{x}_I^n)\,\mathrm{d}\Omega_h\,, \tag{49}$$

$$\mathbf{A}^* = \int_{\Omega_h} \nu\nabla\mathbf{N}_{\mathrm{u}}^{\mathrm{T}}(\mathbf{x}, \mathbf{x}_I^n)\nabla\mathbf{N}_{\mathrm{u}}(\mathbf{x}, \mathbf{x}_I^{n-1})\,\mathrm{d}\Omega_h\,, \tag{50}$$

$$\mathbf{G} = \int_{\Omega_h} \frac{1}{\rho}\mathbf{N}_{\mathrm{u}}^{\mathrm{T}}(\mathbf{x}, \mathbf{x}_I^n)\nabla\mathbf{N}_{\mathrm{p}}(\mathbf{x}, \mathbf{x}_I^{n-1})\mathbf{p}_{\mathrm{X}}^{n-1}\,\mathrm{d}\Omega_h\,, \tag{51}$$

$$\mathbf{R} = \int_{\Omega_h} \mathbf{N}_{\mathrm{u}}^{\mathrm{T}}(\mathbf{x}, \mathbf{x}_I^n)\mathbf{f}(T^{n-1})\,\mathrm{d}\Omega_h\,. \tag{52}$$

In the second step, the first correction of the velocity $\bar{\mathbf{u}}_{\mathrm{X}}^n$ is obtained from

$$\frac{1}{\Delta t}\mathbf{C}\,\bar{\mathbf{u}}_{\mathrm{X}}^n = \frac{1}{\Delta t}\mathbf{C}\,\hat{\mathbf{u}}_{\mathrm{X}}^n + \frac{1}{2}\mathbf{G}^*. \tag{53}$$

The pressure field that satisfies the continuity constrain is calculated in the third step

$$\mathbf{A}_{\mathrm{p}}\mathbf{p}_{\mathrm{X}}^n = \frac{2\rho}{\Delta t}\mathbf{R}_{\mathrm{p}}\,, \tag{54}$$

where

$$\mathbf{A}_{\mathrm{p}} = \int_{\Omega_h} \nabla\mathbf{N}_{\mathrm{p}}^{\mathrm{T}}(\mathbf{x}, \mathbf{x}_I^n)\nabla\mathbf{N}_{\mathrm{p}}(\mathbf{x}, \mathbf{x}_I^n)\,\mathrm{d}\Omega_h\,, \tag{55}$$

$$\mathbf{R}_{\mathrm{p}} = \int_{\Omega_h} \frac{2\rho}{\Delta t}\nabla\mathbf{N}_{\mathrm{p}}^{\mathrm{T}}(\mathbf{x}, \mathbf{x}_I^n)\mathbf{N}_{\mathrm{u}}(\mathbf{x}, \mathbf{x}_I^n)\bar{\mathbf{u}}_{\mathrm{X}}^n\,\mathrm{d}\Omega_h\,. \tag{56}$$

Finally, the velocity at the time step n is obtained from

$$\frac{1}{\Delta t}\mathbf{C}\,\mathbf{u}_{\mathrm{X}}^n = \frac{1}{\Delta t}\mathbf{C}\,\bar{\mathbf{u}}_{\mathrm{X}}^n - \frac{1}{2}\mathbf{G}\,, \tag{57}$$

where

$$\mathbf{G} = \int_{\Omega_h} \frac{1}{\rho}\mathbf{N}_{\mathrm{u}}^{\mathrm{T}}(\mathbf{x}, \mathbf{x}_I^n)\nabla\mathbf{N}_{\mathrm{p}}(\mathbf{x}, \mathbf{x}_I^n)\mathbf{p}_{\mathrm{X}}^n\,\mathrm{d}\Omega_h\,. \tag{58}$$

A fully implicit time approximation scheme is applied to the heat equation (1), [39], which gives

$$\left(\frac{1}{\Delta t}\mathbf{C}_{\mathrm{T}} + \mathbf{B}_{\mathrm{T}} + \mathbf{A}_{\mathrm{T}}\right)\mathbf{T}_{\mathrm{X}}^{n} = -\frac{1}{\Delta t}\mathbf{C}_{\mathrm{T}}^{*}\mathbf{T}_{\mathrm{X}}^{n-1} - \mathbf{R}_{\mathrm{T}}, \tag{59}$$

where

$$\mathbf{C}_{\mathrm{T}} = \int_{\Omega_h} c\mathbf{N}_{\mathrm{T}}^{\mathrm{T}}(\mathbf{x}, \mathbf{x}_I^n)\mathbf{N}_{\mathrm{T}}(\mathbf{x}, \mathbf{x}_I^n)\,\mathrm{d}\Omega_h\,, \tag{60}$$

$$\mathbf{B}_{\mathrm{T}} = \int_{\Omega_h} c\mathbf{N}_{\mathrm{T}}^{\mathrm{T}}(\mathbf{x}, \mathbf{x}_I^n)\mathbf{u}_{\mathrm{X}}^{n}\nabla\mathbf{N}_{\mathrm{T}}(\mathbf{x}, \mathbf{x}_I^n)\,\mathrm{d}\Omega_h\,, \tag{61}$$

$$\mathbf{A}_{\mathrm{T}} = \int_{\Omega_h} k\nabla\mathbf{N}_{\mathrm{T}}^{\mathrm{T}}(\mathbf{x}, \mathbf{x}_I^n)\nabla\mathbf{N}_{\mathrm{T}}(\mathbf{x}, \mathbf{x}_I^n)\,\mathrm{d}\Omega_h\,, \tag{62}$$

$$\mathbf{C}_{\mathrm{T}}^{*} = \int_{\Omega_h} c\mathbf{N}_{\mathrm{T}}^{\mathrm{T}}(\mathbf{x}, \mathbf{x}_I^n)\mathbf{N}_{\mathrm{T}}(\mathbf{x}, \mathbf{x}_I^{n-1})\,\mathrm{d}\Omega_h\,, \tag{63}$$

$$\mathbf{R}_{\mathrm{T}} = \int_{\Omega_h} f\,\mathbf{N}_{\mathrm{T}}^{\mathrm{T}}(\mathbf{x}, \mathbf{x}_I^n)\,\mathrm{d}\Omega_h - \int_{\Gamma_N} q_N\mathbf{N}_{\mathrm{T}}^{\mathrm{T}}(\mathbf{x}, \mathbf{x}_I^n)\,\mathrm{d}\Gamma_N\,. \tag{64}$$

The domain of integration containing the interface is divided into separated sub-regions due to discontinuity of an integrant. One notes that in $\mathbf{C}^{*}$ the integrant is discontinuous at two distinct positions $\mathbf{x}_I^n$ and $\mathbf{x}_I^{n-1}$.

6. Enforcement of the interface conditions

The interface condition for temperature (6) and the no-slip condition for velocity (12) are enforced using the *penalty approach* proposed in [40].

The internal condition (6) can be defined as a penalty function

$$P(T) = T - T_{\mathrm{M}} = 0 \quad \text{at } \Gamma_I\,. \tag{65}$$

Introducing the approximation (36) to the penalty function P gives

$$P(\mathbf{T}_{\mathrm{X}}) = N_{\mathrm{T}}(\mathbf{x}, \mathbf{x}_I)\mathbf{T}_{\mathrm{X}} - T_{\mathrm{M}} = 0 \quad \forall\mathbf{x} \in \Gamma_I\,. \tag{66}$$

For a finite number of points, equation (66) represents a system of linear constraints

$$\mathbf{P}\,\mathbf{T}_{\mathrm{X}} - \mathbf{T}_{\mathrm{M}} = \mathbf{0}, \tag{67}$$

where all the elements of the vector $\mathbf{T}_{\mathrm{M}}$ are equal to T_{M} and the row i of the matrix $\mathbf{P}$ is $\mathbf{N}_{\mathrm{T}}(\mathbf{x}_i, \mathbf{x}_I)$.

The interface temperature is enforced by adding a penalty force

$$\mathbf{f}_{\mathrm{P}} = \alpha_{\mathrm{T}}\mathbf{P}^{\mathrm{T}}\mathbf{P}\mathbf{T}_{\mathrm{X}} - \alpha_{\mathrm{T}}\mathbf{P}^{\mathrm{T}}\mathbf{T}_{\mathrm{M}} \tag{68}$$

to equation (59)

$$\left(\frac{1}{\Delta t}\mathbf{C}_{\mathrm{T}} + \mathbf{B}_{\mathrm{T}} + \mathbf{A}_{\mathrm{T}} + \alpha_{\mathrm{T}}\mathbf{P}^{\mathrm{T}}\mathbf{P}\right)\mathbf{T}_{\mathrm{X}}^{n} = -\frac{1}{\Delta t}\mathbf{C}_{\mathrm{T}}^{*}\mathbf{T}_{\mathrm{X}}^{n-1} - \mathbf{R}_{\mathrm{T}} - \alpha_{\mathrm{T}}\mathbf{P}^{\mathrm{T}}\mathbf{T}_{\mathrm{M}}\,, \tag{69}$$

where α_{T} is the positive constant defining the penalty parameter for the temperature condition.

Similarly, the no-slip condition for velocity (12) is enforced by adding a penalty force

$$\mathbf{f}_{\mathrm{P}} = \alpha_{\mathrm{U}}\mathbf{P}_{\mathrm{u}}^{\mathrm{T}}\mathbf{P}_{\mathrm{u}}\mathbf{u}_{\mathrm{X}} \tag{70}$$

to equations (44), (53) and (57). The row i of the matrix $\mathbf{P}_{\mathrm{u}}$ is $\mathbf{N}_{\mathrm{u}}(\mathbf{x}_i, \mathbf{x}_I)$ while α_{U} is a penalty parameter defined for the velocity constraint.

In the method, the value of the penalty parameter determines the level of satisfaction of the constraint and, on the other hand, the conditioning number of the system.

7. Numerical examples

7.1. Natural convection of water without a phase change

Let us consider natural convection of pure water placed in a differentially heated square-shaped container. The initial temperature $T_0 = 5^{\circ}\mathrm{C}$ and the initial velocity $\mathbf{u}_0 = \mathbf{0}$ m/s are assumed to be uniform. The temperature of the left (hot) and the right (cold) vertical walls are $T_H = 10^{\circ}\mathrm{C}$ and $T_C = 0^{\circ}\mathrm{C}$, respectively. The horizontal walls are assumed to be adiabatic. The no-slip condition is applied for velocity on all the walls. The zero-pressure condition is prescribed at one point. The problem configuration is presented in Fig. 2.

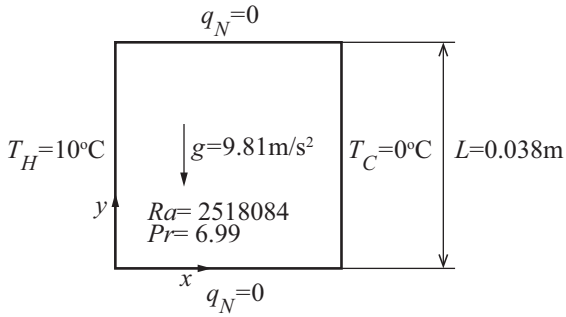

Fig. 2. Natural convection of water – problem definition

The material properties of water used in the numerical model are provided in Table 1. The fourth order polynomial given in [41] was used for the approximation of density in the buoyancy term. The container dimension and the gravitational acceleration are $L = 0.038$ m and $g = 9.81$ m/s, respectively.

Table 1.

Material properties of pure water

ρ_L	c_L	k_L	ν	β (at 0°C)
kg/m^3	Ws/m^{3}K	W/mK	m^2/s	1/K
999.8	4182	0.6	$1.0032 \cdot 10^{-6}$	$6.734 \cdot 10^{-5}$

The dimensionless parameters defining the problem are the Rayleigh and Prandl numbers, $\mathrm{Ra} = g\beta c_L(T_H - T_C)L^3/k_L\nu = 2518084$ and $\mathrm{Pr} = \nu c_L/k_L = 6.99$, respectively.

The steady-state solution is assumed to have been reached when the L_2 norm of the velocity residual has a value below 0.1%. The L_2 norm is calculated as

$$L_2 = \frac{\left\|\mathbf{u}^n - \mathbf{u}^{n-1}\right\|}{\|\mathbf{u}^n\|} \cdot 100\%. \tag{71}$$

Figs 3 and 4 present the steady-state solution for the velocity and temperature profiles along the horizontal and vertical symmetry lines obtained using irregular 50×50 and 100×100 element meshes and time steps $\Delta t = 2.5$ s and $\Delta t = 0.5$ s. The non-dimensional coordinates are used.

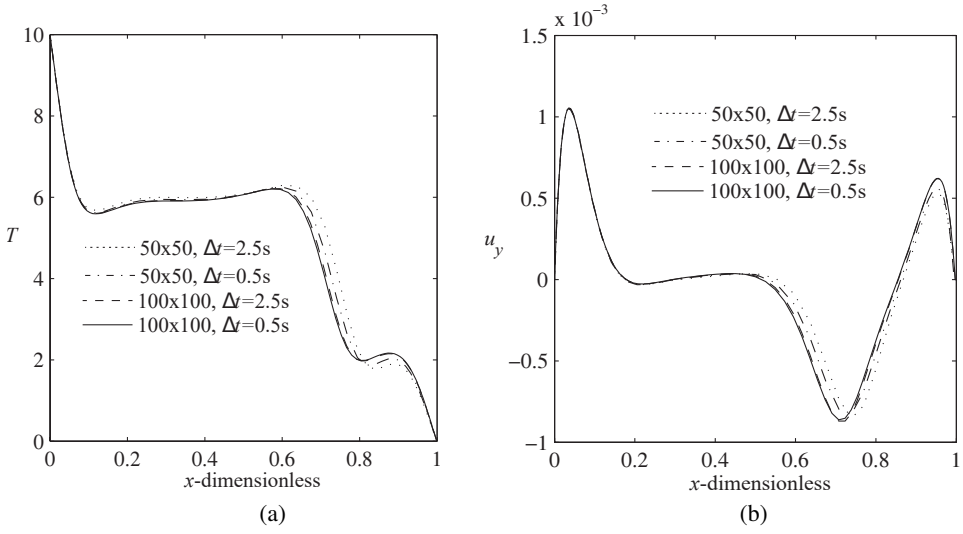

Fig. 3. Profile of temperature a) and y-velocity component b) along the horizontal symmetry line

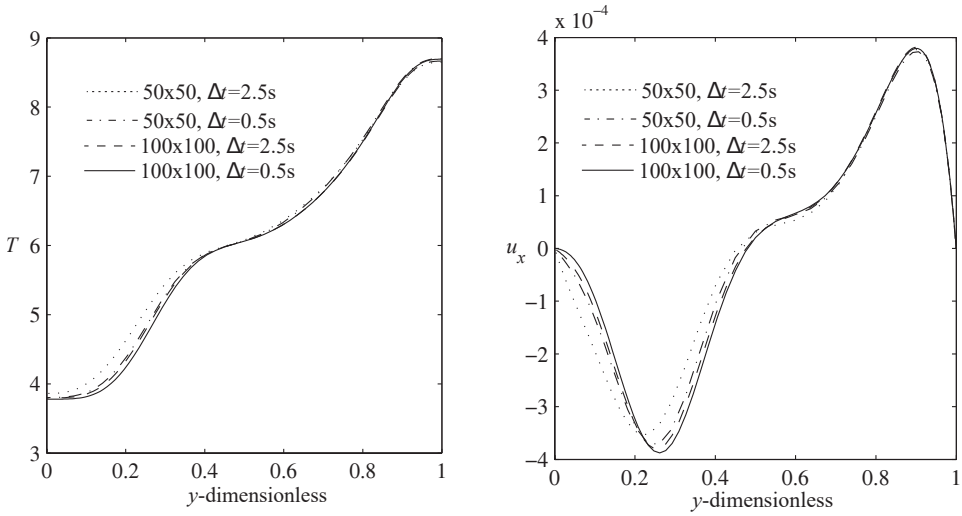

Fig. 4. Profile of temperature a) and x-velocity component b) along the vertical symmetry line

The results seem to be in good agreement with those obtained by Michalek & Kowalewski (see Figs 1 and 3 in [42]), who employed the finite volume method and the finite difference method, and Danaila et al., who applied the adaptive finite element method (see Fig. 6 in [9]). The steady-state solution is used as the initial condition for the freezing problem.

7.2. Water freezing with natural convection

The problem considered above is the starting point for the analysis of water freezing in a square-shaped container. The water begins to freeze after the temperature of the right wall T_C drops rapidly from 0°C to −10°C. The steady-state patterns obtained in the previous example are used as the initial conditions for the temperature, velocity and pressure fields.

The thermophysical properties, melting temperature and latent heat of ice used in the numerical model are provided in Table 2. The thermophysical properties of water remain unchanged.

Table 2.

Material properties of ice

ρ_S	c_S	k_S	T_M	ℓ^p
kg/m^3	Ws/m^{3}K	W/mK	°C	Ws/kg
916.8	2116	2.26	0	$335{\cdot}10^3$

A 50×50 element mesh and a time step of 0.5 s were used in the calculations. The penalty parameters for the temperature and velocity conditions are defined as

$\alpha_T = 10^8$ and $\alpha_U = 1$, respectively. The position of the ice/water interface and the recirculation pattern for $t = 100$ s and $t = 300$ s counted from the moment water started freezing are shown in Fig. 5. The profiles of velocity and temperature along the horizontal symmetry line are presented in Fig. 6. The results are compared with those obtained by means of the commercial codes FLUENT 6.0 and NC4MARV2 used by Michalek & Kowalewski [42]. The experimental data used in the test are those obtained by Giangi et al. [43].

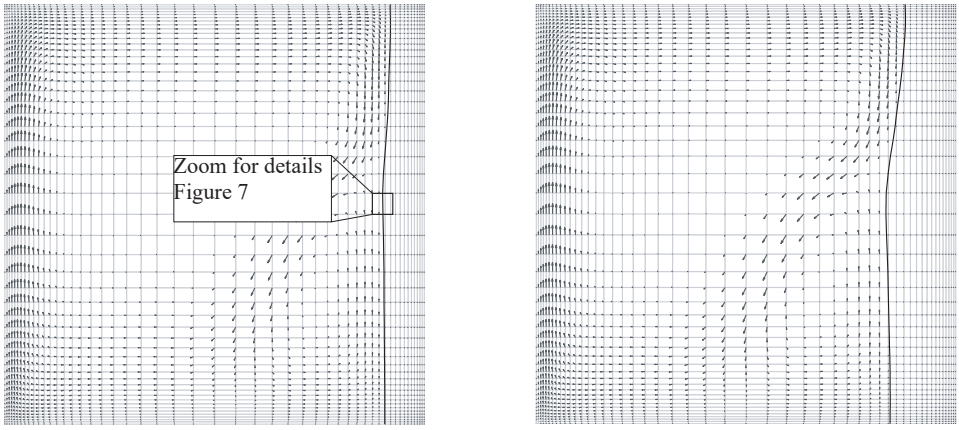

(a) (b)

Fig. 5. Recirculation pattern and the position of the interface front for $t = 100$ s and $t = 300$ s

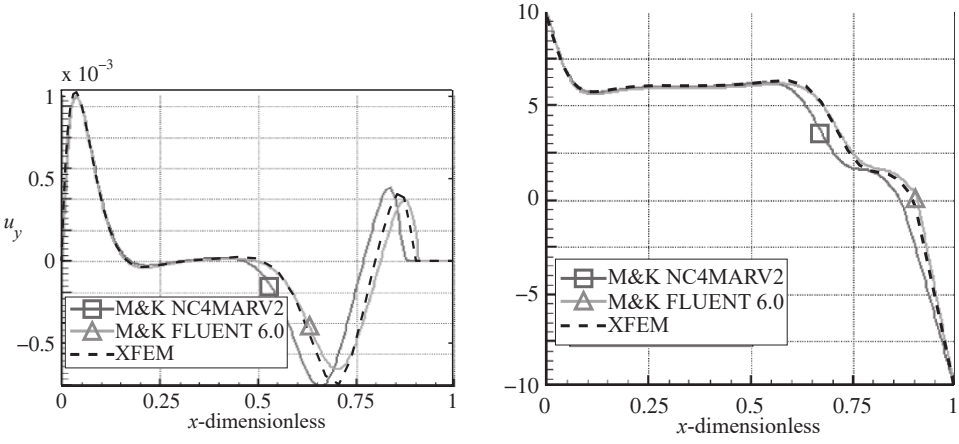

(a) (b)

Fig. 6. Profile of the y-velocity component a) and temperature b) along the horizontal symmetry line for $t = 100$ s

Fig. 7 shows zoomed-in view of the approximation of the discontinuity in the velocity, temperature and pressure fields for the element cut by the interface, see Fig. 5a. As can be seen, the approximation of the element allows for a kink in the velocity and temperature fields and a jump in the pressure field along the interface line, without any unphysical oscillations, which can be observed for the standard XFEM approaches, [44].

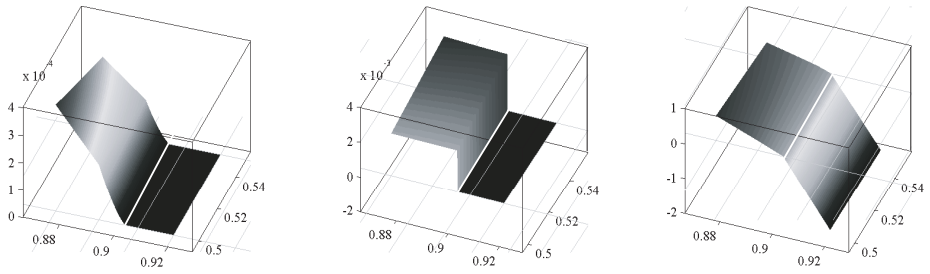

(a) (b) (c)

Fig. 7. Zoomed-in view for the area shown in Fig. 5a: a) velocity, b) pressure and c) temperature

7.3. Melting of a phase change material (PCM)

The problem considered in this section is the melting of n-octadecane, a PCM, involving natural convection in a square cavity. The physical model of the test is shown in Fig. 8. Specific heat and conductivity are assumed to be different for the two phases. Initially, the material is solid ($T_0 = 27.448^\circ$C) but after the left boundary reaches the hot temperature $T_H = 32.745^\circ$C, it starts to melt. The right side is held at cold temperature $T_C = 27.45^\circ$C. The thermophysical properties of n-octadecane defined for the test are presented in Table 3; the data are available from [45]. The

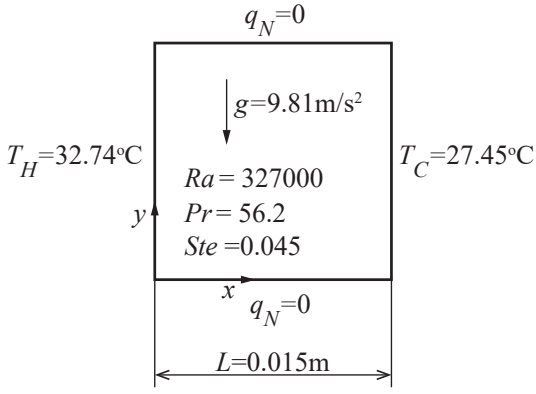

Fig. 8. Melting of the phase change material (n-octadecane). Problem definition

dimensionless parameters describing the test case are the Rayleigh, Prandl and Stefan numbers: $\mathrm{Ra} = g\beta c_L(T_H - T_C)L^3/k_L\nu = 327000$, $\mathrm{Pr} = \nu c_L/k_L = 56.2$ and $\mathrm{Ste} = c_L(T_H - T_C)/\ell = 0.045$, respectively.

Table 3.

Thermophysical properties of n-octadecane

Property	Liquid phase	Solid phase
Density, ρ (kg/m^3)	774	814
Heat capacity, c (kWs/m^{3}K)	1687	1750
Heat conductivity, k (W/m K)	0.152	0.358
Kinematic viscosity, ν (m^2/s)	$5.063{\cdot}10^{-6}$	
Thermal expansion, β (1/K)	$8.5{\cdot}10^{-4}$	
Latent heat, ℓ (Ws/m^3)	$1.986{\cdot}10^{8}$	
Melting point, T_M (°C)	27.5	

Okada [46] investigates the problem both experimentally and numerically using finite difference method coupled with the deforming grid scheme and the variable transformation technique. In [47], the authors solve this problem by applying the temperature transforming model and various solid velocity correction schemes. The solution to the problem proposed by Wang et al. [7] involves employing the finite volume approach and the temperature transforming model. Danaila et al. [9], on the other hand, suggest using the adaptive finite element method.

In this study, the problem was solved using regular and irregular 50×50 element meshes with the time step $\Delta t = 0.1$ s. Fig. 9 presents the positions of the solid–liquid

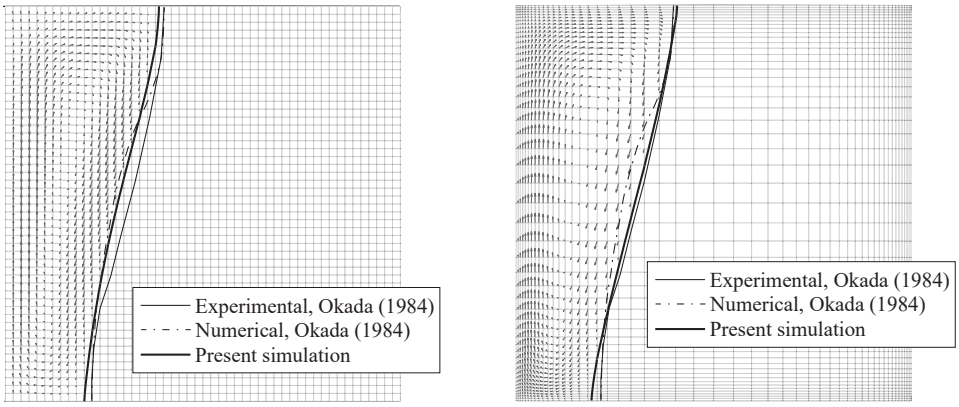

(a) (b)

Fig. 9. Melting of the phase change material (n-octadecane): a) regular 50 × 50 element mesh, b) irregular 50 × 50 element mesh

interface and the natural recirculation pattern for $t = 1794$ s (dimensionless time: $\tau = \dfrac{\alpha_L \cdot \mathrm{Ste} \cdot t}{L^2} = 0.032$). The calculated position of the interface front correlates with the experimental and numerical results [46].

8. Conclusions

This paper has considered the use of a comprehensive numerical model to deal with problems of a phase change with natural convection in liquids. A single-domain approach has been presented and validated for selected phase change systems. The key ingredient of this approach is the use of the extended finite element method and proper approximation of the discontinuity in the physical fields. A new set of enrichment functions has been introduced for the considered problem in a two-dimensional space. The proposed single-mesh approach can accurately represent the discontinuity in the velocity, pressure and temperature fields without re-meshing or moving mesh algorithms.

Three cases have been analysed to illustrate the effectiveness of the proposed method. The first is the classical problem of natural convection of water in a square cavity with no melting involved. The second problem is the natural convection freezing of water and the third example involves melting of a PCM. The main reason for selecting these examples is that they have been broadly studied in the literature, and thus provide the benchmarks for the proposed method. The results obtained from this study seem to be in good agreement with the data reported by other investigators and allows for smooth approximation near the interface boundary.

Manuscript received by Editorial Board, May 21, 2019;
final version, July 10, 2019.

References

[1] A. Faghri and Y. Zhang. *Transport Phenomena in Multiphase Systems*. Elsevier, 2006.

[2] S.C. Gupta. *The Classical Stefan Problem: Basic Concepts, Modelling and Analysis*. Elsevier, 2003.

[3] V. Alexiades and S.D. Solomon. *Mathematical Modeling of Melting and Freezing Processes*. Hemisphere Publ. Co, Washington DC, 1993.

[4] O.C. Zienkiewicz, R.L. Taylor, and P. Nithiarasu. *The Finite Element Method for Fluid Dynamics*, 6th edition. Elsevier Butterworth-Heinemann, Burlington, 2005.

[5] K. Morgan. A numerical analysis of freezing and melting with convection. *Computer Methods in Applied Mechanics and Engineering*, 28(3):275–284, 1981. doi: 10.1016/0045-7825(81)90002-5.

[6] J. Mackerle. Finite elements and boundary elements applied in phase change, solidification and melting problems. A bibliography (1996–1998). *Finite Elements in Analysis and Design*, 32(3):203–211, 1999. doi: 10.1016/S0168-874X(99)00007-4.

[7] S. Wang, A. Faghri, and T.L. Bergman. A comprehensive numerical model for melting with natural convection. *International Journal of Heat and Mass Transfer*, 53(9-10):1986–2000, 2010. doi: 10.1016/j.ijheatmasstransfer.2009.12.057.

[8] G. Vidalain, L. Gosselin, and M. Lacroix. An enhanced thermal conduction model for the prediction of convection dominated solid–liquid phase change. *International Journal of Heat and Mass Transfer*, 52(7-8):1753–1760, 2009. doi: 10.1016/j.ijheatmasstransfer.2008.09.020.

[9] I. Danaila, R. Moglan, F. Hecht, and S. Le Masson. A Newton method with adaptive finite elements for solving phase-change problems with natural convection. *Journal of Computational Physics*, 274:826–840, 2014. doi: 10.1016/j.jcp.2014.06.036.

[10] J.M. Melenk and I. Babuska. The partition of unity finite element method: basic theory and application, *Computer Methods in Applied Mechanics and Engineering*. 139(1-4):289–314, 1996. doi: 10.1016/S0045-7825(96)01087-0.

[11] A. Cosimo, V. Fachinotti, and A. Cardona. An enrichment scheme for solidification problems. *Computational Mechanics*, 52(1):17–35, 2013. doi: 10.1007/s00466-012-0792-9.

[12] T. Belytschko and T. Black. Elastic crack growth in finite elements with minimal remeshing. *International Journal for Numerical Methods in Engineering*, 45(5):601–620, 1999. doi: 10.1002/(SICI)1097-0207(19990620)45:5<601::AID-NME598>3.0.CO;2-S.

[13] R. Merle and J. Dolbow. Solving thermal and phase change problems with the eXtended finite element method. *Computational Mechanics*, 28(5):339–350, 2002. doi: 10.1007/s00466-002-0298-y.

[14] J. Chessa, P. Smolinski, and T. Belytschko. The extended finite element method (XFEM) for solidification problems. *International Journal for Numerical Methods in Engineering*, 53(8):1959–1977, 2002. doi: 10.1002/nme.386.

[15] P. Stapór. The XFEM for nonlinear thermal and phase change problems. *International Journal of Numerical Methods for Heat & Fluid Flow*, 25(2):400–421, 2015. doi: 10.1108/HFF-02-2014-0052.

[16] N. Zabaras, B. Ganapathysubramanian, and L. Tan. Modelling dendritic solidification with melt convection using the extended finite element method. *Journal of Computational Physics*, 218(1):200–227, 2006. doi: 10.1016/j.jcp.2006.02.002.

[17] P. Stapór. A two-dimensional simulation of solidification processes in materials with thermo-dependent properties using XFEM. *International Journal of Numerical Methods for Heat & Fluid Flow*, 26(6):1661–1683, 2016. doi: 10.1108/HFF-01-2015-0018.

[18] J. Chessa and T. Belytschko. An enriched finite element method and level sets for axisymmetric two-phase flow with surface tension. *International Journal for Numerical Methods in Engineering*, 58(13):2041–2064, 2003. doi: 10.1002/nme.946.

[19] J. Chessa and T. Belytschko. An extended finite element method for two-phase fluids. *Journal of Applied Mechanics*, 70(11):10–17, 2003. doi: 10.1115/1.1526599.

[20] M. Li, H. Chaouki, J. Robert, D. Ziegler, D. Martin, and M. Fafard. Numerical simulation of Stefan problem with ensuing melt flow through XFEM/level set method. *Finite Elements in Analysis and Design*, 148:13–26, 2018. doi: 10.1016/j.finel.2018.05.008.

[21] D. Martin, H. Chaouki, J. Robert, D. Ziegler, and M. Fafard. A XFEM phase change model with convection. *Frontiers in Heat and Mass Transfer*, 10:1-11, 2018. doi: 10.5098/hmt.10.18.

[22] S. Osher and J.A. Sethian. Fronts propagating with curvature dependent speed: Algorithms based on Hamilton–Jacobi formulations. *Journal of Computational Physics*, 79(1):12–49, 1988. doi: 10.1016/0021-9991(88)90002-2.

[23] M. Stolarska, D.L. Chopp, N. Möes, and T. Belytschko. Modelling crack growth by level sets in the extended finite element method. *International Journal for Numerical Methods in Engineering*, 51(8):943–960, 2001. doi: 10.1002/nme.201.

[24] M. Sussman, P. Smereka, and S. Osher. A level set approach for computing solutions to incompressible two-phase flow. *Journal of Computational Physics*, 114(1):146–159, 1994. doi: 10.1006/jcph.1994.1155.

[25] M.Y. Wang, X. Wang, and D. Guo. A level set method for structural topology optimization. *Computer Methods in Applied Mechanics and Engineering*, 192(1-2):227–246, 2003. doi: 10.1016/S0045-7825(02)00559-5.

[26] N. Peters. *Turbulent Combustion*. Cambridge University Press, Cambridge, 2000.

[27] Y.H. Tsai and S. Osher. Total variation and level set methods in image science. *Acta Numerica*, 14:509–573, 2005. doi: 10.1017/S0962492904000273.

[28] V. Alexiades and J.B. Drake. A weak formulation for phase-change problems with bulk movement due to unequal densities. In J.M. Chadam and H. Rasmussen editors, *Free Boundary Problems Involving Solids*, pages 82–87, CRC Press, 1993.

[29] S. Chen, B. Merriman, S. Osher, and P. Smereka. A simple level set method for solving Stefan problems. *Journal of Computational Physics*, 135(1):8–29, 1997. doi: 10.1006/jcph.1997.5721.

[30] H. Sauerland. *An XFEM Based Sharp Interface Approach for Two-Phase and free-Surface Flows*. Ph.D. Thesis, RWTH Aachen University, Aachen, Germany, 2013.

[31] J.E. Tarancòn, A. Vercher, E. Giner, and F.J. Fuenmayor. Enhanced blending elements for XFEM applied to linear elastic fracture mechanics. *International Journal for Numerical Methods in Engineering*, 77(1):126–148, 2009. doi: 10.1002/nme.2402.

[32] T.P. Fries. A corrected XFEM approximation without problems in blending elements. *International Journal for Numerical Methods in Engineering*, 75(5):503–532, 2008. doi: 10.1002/nme.2259.

[33] N. Moës, M. Cloirec, P. Cartraud, and J.F. Remacle. A computational approach to handle complex microstructure geometries. *Computer Methods in Applied Mechanics and Engineering*, 192(28-30):3163–3177, 2003. doi: 10.1016/S0045-7825(03)00346-3.

[34] G. Zi and T. Belytschko. New crack-tip elements for XFEM and applications to cohesive cracks. *International Journal for Numerical Methods in Engineering*, 57(15):2221–2240, 2003. doi: 10.1002/nme.849.

[35] G. Ventura, E. Budyn, and T. Belytschko. Vector level sets for description of propagating cracks in finite elements. *International Journal for Numerical Methods in Engineering*, 58(10):1571–1592, 2003. doi: 10.1002/nme.829.

[36] P. Stąpór. An improved XFEM for the Poisson equation with discontinuous coefficients. *Archive of Mechanical Engineering*, 64(1):123–144, 2017. doi: 10.1515/meceng-2017-0008.

[37] H.G. Choi, H. Choi, and J.Y. Yoo. A fractional four-step finite element formulation of the unsteady incompressible Navier-Stokes equations using SUPG and linear equal-order element methods. *Computer Methods in Applied Mechanics and Engineering*, 143(3-4):333–348, 1997. doi: 10.1016/S0045-7825(96)01156-5.

[38] R. Codina. Pressure stability in fractional step finite element methods for incompressible flows. *Journal of Computational Physics*, 170(1):112–140, 2001. doi: 10.1006/jcph.2001.6725.

[39] Z. Chen. *Finite Element Methods and Their Applications*. Springer, 2005.

[40] T. Belytschko, W.K. Liu, and B. Moran. *Nonlinear Finite Elements for Continua and Structures*. Wiley, 2000.

[41] T.A. Kowalewski and M. Rebow. Freezing of water in differentially heated cubic cavity. *International Journal of Computational Fluid Dynamics*, 11(3-4):193–210, 1999. doi: 10.1080/10618569908940874.

[42] T. Michałek and T.A. Kowalewski. Simulations of the water freezing process – numerical benchmarks. *Task Quarterly*, 7(3):389–408, 2003.

[43] M. Giangi, T.A. Kowalewski, F. Stella, and E. Leonardi. Natural convection during ice formation: numerical simulation vs. experimental results. *Computer Assisted Mechanics and Engineering Sciences*, 7(3):321–342, 2000.

[44] P. Stąpór. An enhanced XFEM for the discontinuous Poisson problem. *Archive of Mechanical Engineering*, 66(1):25–37, 2019. doi: 10.24425/ame.2019.126369.

[45] *Thermal-FluidCentral. Thermophysical Properties: Phase Change Materials*, 2010 (last accessed January 14, 2016). https://thermalfluidscentral.org.

[46] M. Okada. Analysis of heat transfer during melting from a vertical wall. *International Journal of Heat and Mass Transfer*, 27(11):2057–2066, 1984. doi: 10.1016/0017-9310(84)90192-3.

[47] Z. Ma and Y. Zhang. Solid velocity correction schemes for a temperature transforming model for convection phase change. *International Journal of Numerical Methods for Heat & Fluid Flow*, 16(2):204–225, 2006. doi: 10.1108/09615530610644271.